Cancer Spheroids: Super-Resolution Mapping of Single Nanoparticles inside Tumor Spheroids (Small 6/2020)

Article *in* Small · February 2020

DOI: 10.1002/smll.202070030

11 authors, including:

Yongtao Liu
University of Technology Sydney
20 PUBLICATIONS **102** CITATIONS
SEE PROFILE

Fan Wang
University of Technology Sydney
113 PUBLICATIONS **2,453** CITATIONS
SEE PROFILE

Hongxu Lu
University of Technology Sydney
90 PUBLICATIONS **2,633** CITATIONS
SEE PROFILE

Guocheng Fang
University of Technology Sydney
17 PUBLICATIONS **108** CITATIONS
SEE PROFILE

NANO · MICRO small
www.small-journal.com

Super-Resolution Mapping of Single Nanoparticles inside Tumor Spheroids

Yongtao Liu, Fan Wang, Hongxu Lu, Guocheng Fang, Shihui Wen, Chaohao Chen, Xuchen Shan, Xiaoxue Xu, Lin Zhang, Martina Stenzel, and Dayong Jin*

Cancer spheroids have structural, functional, and physiological similarities to the tumor, and have become a low-cost in vitro model to study the physiological responses of single cells and therapeutic efficacy of drugs. However, the tiny spheroid, made of a cluster of high-density cells, is highly scattering and absorptive, which prevents light microscopy techniques to reach the depth inside spheroids with high resolution. Here, a method is reported for super-resolution mapping of single nanoparticles inside a spheroid. It first takes advantage of the self-healing property of a "nondiffractive" doughnut-shaped Bessel beam from a 980 nm diode laser as the excitation, and further employs the nonlinear response of the 800 nm emission from upconversion nanoparticles, so that both excitation and emission at the near-infrared can experience minimal loss through the spheroid. These strategies lead to the development of a new nanoscopy modality with a resolution of 37 nm, 1/26th of the excitation wavelength. This method enables mapping of single nanoparticles located 55 µm inside a spheroid, with a resolution of 98 nm. It suggests a solution to track single nanoparticles and monitor their release of drugs in 3D multicellar environments.

Tumor spheroids are the engineered cell clusters in 3D space. Compared with the cells cultured on Petri dish, the spheroid model provides the natural physiological environment for live cells, which facilitate the interaction of the living cells with other cells and cellular matrix.[1,2] Therefore, this model fills the gap between the in vivo animal tests and in vitro 2D culture for high-throughput, low-cost study of cell behaviors in a living organism,[3] and treatment efficacy. To study the intractable single cell behaviors and drug delivery process inside the spheroids, optical microscopy[4,5] provides great potentials, which have already displayed the super-resolution imaging abilities for various biology system.[6] However, the cell density of spheroid is usually much higher than the conventional biological tissue, which results in much stronger scattering and absorption for both excitation and emission light. The scattering distorts the excitation wavefront and decreases imaging resolution.

To achieve optical imaging inside deep tissue, the near-infrared (NIR) window is an ideal range for light excitation and emission to avoid the strong tissue absorption.[7] In 2003, Patrick et al. first employed the NIR light as the excitation beam in two-photon microscopy to reduce the tissue scattering for deep tissue imaging. In vivo study showed that two-photon fluorescence images can be obtained throughout almost the entire gray matter of a mouse neocortex (up to 1 mm depth).[8] In 2017, dual NIR two-photon microscopy was proposed, which reduces the light scattering by eight times compared to conventional one-photon excitation microscopy.[9] Gratton's group studied the penetration ability of the NIR light (wavelength 650–1000 nm) in human breast tumors.[10] They showed that with a superior tissue penetration ability the NIR light can be used for noninvasively breast cancer detection. Rosenthal's group shows NIR light can be used to image human breast cancer flank xenografts with the imaging depth of 5–10 mm.[11] Apart from the deep tissue penetration abilities, NIR light is also less phototoxic compared to the visible light, owing to the lack of significant endogenous (one-photon) absorbers in most tissues.[12]

Upconversion nanoparticles (UCNPs), consisting of sensitizer ions (e.g., ytterbium Yb^{3+}) and emitter ions (e.g., thulium Tm^{3+}), could convert low-energy NIR photons to high-energy photons. The anti-Stokes luminescence and nonlinear saturation excitation characteristics are promising for background-free biosensing and bioimaging. Also, UCNPs have been demonstrated as excellent nanoprobes for super-resolution subcellular imaging[13–15] at low excitation power. Most recently, we developed a new mode of NIR emission saturation[16] nanoscopy for deep tissue super-resolution imaging, where both the 980 nm excitation beam and 800 nm emission beam locate at the transparent biological window, achieving long penetration depth. The next challenge

Y. Liu, Dr. F. Wang, G. Fang, Dr. S. Wen, C. Chen, X. Shan, Dr. X. Xu, Prof. D. Jin
Institute for Biomedical Materials and Devices (IBMD)/Faculty of Science
University of Technology Sydney
Sydney, NSW 2007, Australia
E-mail: fan.wang@uts.edu.au

Dr. H. Lu, L. Zhang, Prof. M. Stenzel
School of Chemistry/Centre for Advanced Macromolecular Design (CAMD)
University of New South Wales
Kensington, Sydney, NSW 2052, Australia

Prof. D. Jin
UTS-SUStech Joint Research Centre for Biomedical Materials & Devices
Southern University of Science and Technology
Shenzhen, Guangdong 518055, P. R. China

The ORCID identification number(s) for the author(s) of this article can be found under https://doi.org/10.1002/smll.201905572.

DOI: 10.1002/smll.201905572

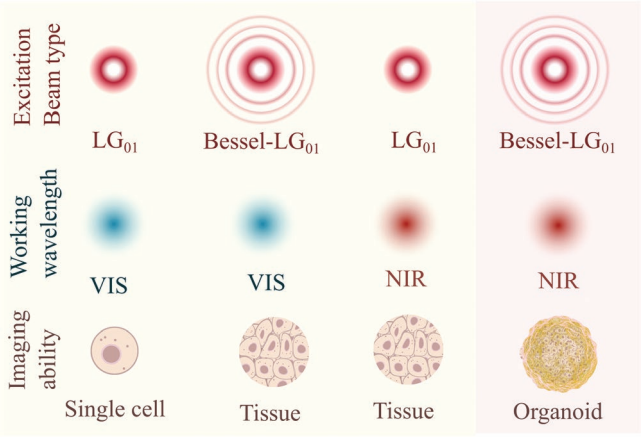

Figure 1. The schematic of deep tissue imaging ability by a different type of excitation beams. LG01: Laguerre–Gaussian (LG_{01}) beam; B-LG_{01}: Bessel–Laguerre–Gaussian (B-LG_{01}) beam; VIS: visible; NIR: near-infrared. The imaging ability shows the suitable biological sample for different types of excitation beam with certain working wavelength. LG_{01} beam with VIS wavelength (LG_{01}-VIS) is good for super-resolution imaging of single cells. Either B-LG_{01}-VIS or LG_{01}-NIR could be used for super-resolution imaging through tissue (up to around 100 µm). B-LG_{01}-NIR can be used for super-resolution imaging in organoid.

for super-resolution imaging is to mitigate the strong scattering and resolve nanoscale features inside spheroids.

In this work, by introducing Bessel beam, we demonstrated an NIR Bessel-beam emission saturation nanoscopy (NIRB) as a solution for super-resolved nanoparticle imaging inside a spheroid, with robust single beam setup, low excitation power, and high resolution. The developed NIRB can overcome the scattering from multicellular spheroids and maintain sub-100 nm full width at half maximum (FWHM) over 50 µm depth inside a spheroid.

For deep tissue super-resolution imaging, the scattering and absorption significantly limit the imaging depth and the resolution. Applying visible Laguerre–Gaussian (LG_{01}-VIS) beam, the conventional scanning nanoscopy requires ultrahigh peak excitation power (e.g., 9.4×10^3 MW cm^{-2})[17] to balance the tissue's scattering and absorption based on visible excitation and emission to achieve high resolution inside the tissues (**Figure 1**). The Bessel beam, so-called "nondiffractive" beam, is an interference created beam, which can be regarded as the coherent superposition of many plane wavelet with flat wavefront for one azimuthal angle. As a result, few scattered wavelets would not affect the focus quality of the Bessel beam. Adopting from this "nondiffractive" Bessel beam, Bessel-LG01 (B-LG_{01}-VIS) nanoscopy can moderate the scattering from biological tissue,[18,19] achieving better imaging depth. However, the visible excitation and emission limit the imaging depth in the biological system. An NIR LG_{01} (LG_{01}-NIR) excitation beam, together with NIR emission, minimizes sample absorption, achieving good resolution inside deep tissue at relatively low excitation power.[16] Taking advantage from both Bessel beam and NIR excitation and emission of UCNPs, the NIRB nanoscopy will simultaneously tackle the problems in light absorption and scattering for resolving single nanoparticles in the spheroids.

UCNPs doped with Tm^{3+} and Yb^{3+} are employed as fluorescence probe in this study, due to their excitation and emission located at the NIR biological window. Figure S14a,b of the Supporting Information is the TEM image and the size distribution of the UCNPs, respectively. These UCNPs are of high uniformity in particle size (87.9 ± 5 nm). The synthesizing process is shown in Note S1 of the Supporting Information. Figure S14c of the Supporting Information shows the energy levels diagram of the sensitizer (Yb^{3+}) and emitter (Tm^{3+}) in UCNPs, where Yb^{3+} can directly absorb the 980 nm NIR photons and pump ground state electrons to the excited state. Benefiting from this linear absorption, UCNPs have larger absorption cross-section compared with conventional two-photon imaging probe.[16] Through the energy transfer process,[20,21] the sensitizer can transfer their energy to the emitter, pumping electrons in the multi-intermediate ladder-like energy levels of the Tm^{3+} to higher excited states. These process efficiently upconverts excited NIR excitation photon to visible and NIR emissions. Their emission intensity is comparable with quantum dot.[13] In this study, Tm^{3+} emitters are employed to get the 800 nm emission with their lower two-photon energy state $^3H_4$ (Figure S14c, Supporting Information). Figure S14d of the Supporting Information shows the typical emission spectrum of a single UCNP. Under 980 nm excitation, the photon energy will be transferred to the excited energy levels in Tm^{3+}, producing strong emissions at 455, 475, 650, and 800 nm. As both the 800 nm emission and 980 nm excitation locate at the NIR biological window,[16] we apply this nanoprobe into NIRB nanoscopy to minimize the absorption from the spheroid. The excitation-power-dependent emission property at 800 nm is shown in Figure S14e of the Supporting Information, where the emission shows a unique nonlinear saturation, which enables the designing of saturation based super-resolution technology. These UCNPs are highly uniform emission intensity (see Note S2, Supporting Information), which provides good imaging repeatability.[15,22,23]

Figure 2a shows a schematic of the optical system for NIRB, which applies a Bessel-LG_{01} (B-LG_{01}) excitation beam with a wavelength of 976.5 nm. Adopting the "nondiffractive" ability from the Bessel beam, the B-LG_{01} excitation beam enables NIRB to address the issue of light scattering. Figure 2b illustrates this "nondiffractive" ability. Bessel beam is an interference type of beam that can be regarded as the coherent superposition of many plane wavelet with equal amplitudes. An obstacle in the beam pass will block some wavelets, the light field around the obstacle will be disrupted. While when the beam is further propagating, the other wavelets that have parallel propagation direction will interfere with each other to form the new "cured" focus along the optical axis. For instance, as shown in the simulation (Figure 2b), the B-LG_{01} beam can maintain its focus profile even with a 500 nm diameter bead sits 250 nm off from its optical axis to scatter the beam. This B-LG_{01} has a doughnut-shaped profile at the focus plane, and the super-resolution image is generated by scanning this B-LG_{01} across the sample. During the scanning, when a single UCNP is placed in the middle of the doughnut profile, it comes across minimized excitation power, thereby generating a doughnut-shaped emission pattern with a dip at the position where the UCNP sits. Hence, each of UCNP shows a doughnut point spread function (PSF) in the NIRB image, as shown in the inset of Figure 2b. The FWHM of the dip at PSF is defined as the resolution of NIRB, refer to other LG_{01} beam-based nanoscopy.[24] We compare the confocal image with

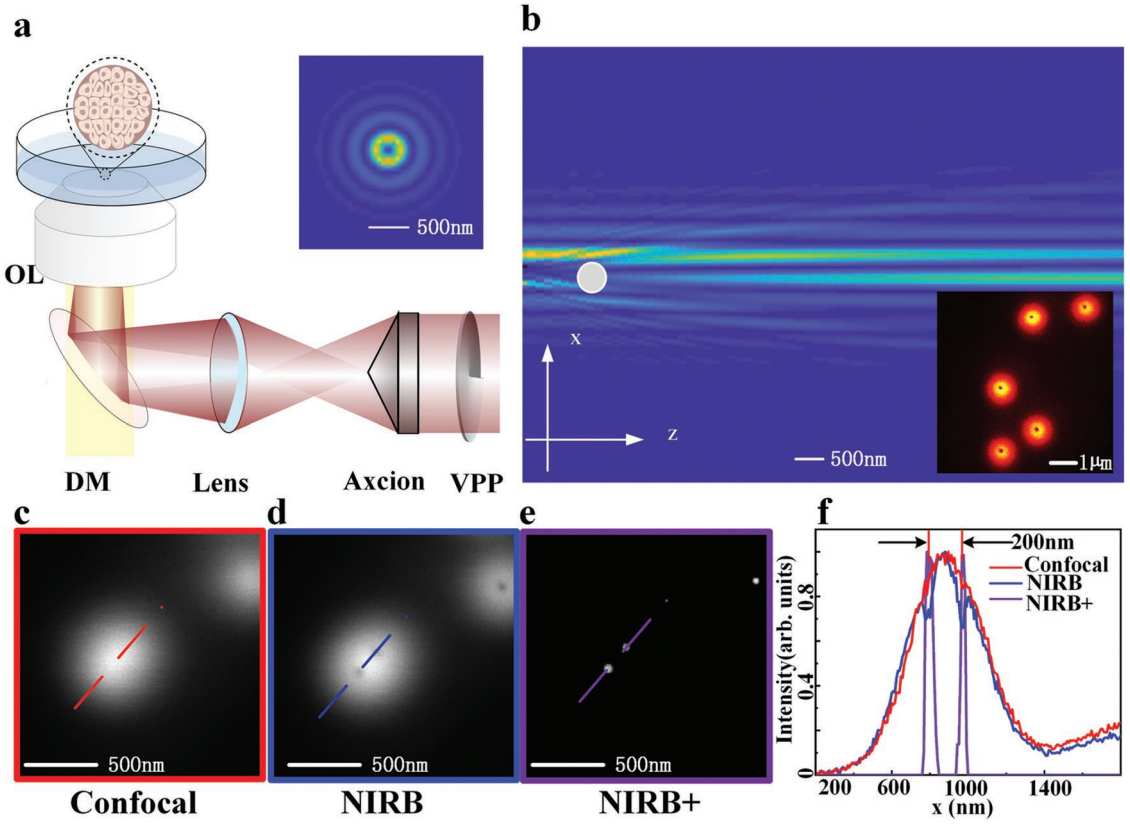

Figure 2. a) Schematic of the NIRB nanoscopy setup (details show in Note S3, Supporting Information). The Bessel-doughnut beam is created by directing a Gaussian beam go through a vortex phase plate (VPP) and an Axicon lens, then focusing into the focus plane by a high NA objective lens (NA 1.4), DM is a dichroic mirror, and OL is the objective lens. The inset is the calculated *x*–*y* cross-section of the Bessel beam. b) The calculated *x*–*z* cross-section of Bessel beam, scattered by a 500 nm diameter bead with 250 nm off from its optical axis. The *x*–*y* plane is imaging plan, *z*-direction is beam propagation direction. The inset is an NIRB image of free dispersed UCNPs in water solution under excitation of 5.44 MW cm^{-2}. c) Confocal image of UCNPs by detecting 800 nm emission. d) Raw NIRB image corresponding to (f). e) The positive NIRB image (NIRB+) after data process. f) The cross-section profile of UCNPs from the confocal, NIRB and NIRB+ images, respectively. The pixel dwell time for NIRB is 3 ms.

NIRB image of two overlapped UCNPs in Figure 2c–f. NIRB is able to resolve the two UCNPs that cannot be distinguished by confocal microscopy. The positive NIRB image (NIRB+) can be calculated through the deconvolution process. Figure 2f shows the crossline profile of the UCNPs images in Figure 2c–e.

The resolution of NIRB could be optimized by tuning the excitation power. **Figure 3**a shows the PSF of single UCNP for different excitation power. Under 10 mW excitation power, the resolution (≈262 nm) is still inferior to the conventional diffraction imitated resolution (200 nm). According to the nonlinear saturation curve (Figure S14e, Supporting Information) of UCNP, high power excitation doughnut PSF will generate a saturated doughnut PSF that indicates a reduced FHWM in the dip of PSF. With the power of 100 mW, the FWHM is below 100 nm (≈1/10th of the excitation wavelength), beyond diffraction limitation. When the excitation power is higher than 140 mW, the dip of the PSF subjects to saturation, and the PSF for 240 mW show a Gaussian profile that provides an alternative way to generate a positive image than deconvolution.[25] It is notable that different doping concentration in UCNP results in different saturation curve and the resultant optical resolution. Three features from the saturation curve affect the resolution: 1) the power point (I_S) to achieve the half value of the maximum intensity; 2) the power point (I_{MAX}) to achieve maximum intensity; 3) the power point (I_{on}) to achieve e^{-2} of the maximum emission intensity. Lower values of I_S and/or I_{MAX} will provide narrower dip of the emission PSF, which increases the resolution. The increase of the I_{on} will decrease the dip intensity thereby enhancing the resolution. According to our previous result,[15] 4% Tm^{3+}-doped UCNPs showed the excellent power-dependent emission curve and has been selected as the imaging probe for NIRB. Figure 3b shows the power dependent resolution of NIRB imaging on a single UCNP doped with 4% Tm^{3+} and 20% Yb^{3+}. Generally, the higher excitation power applied to the particle could achieve a better resolution. However, higher excitation power also increases the dip height in the PSF, which seriously affect the signal to noise ratio when the dip intensity is more than 50% of the maximum intensity. Hence, there is an optimized excitation power to achieve the best resolution. With excitation power of 10.88 MW cm^{-2}, we achieved an optimized resolution of 37 nm (1/26th of the excitation wavelength), as shown in the inset of Figure 3b. Figure 3c,d shows the NIRB and NIRB+ images of two UCNPs. According to the crossline profile of UCNPs' image (Figure 3e), NIRB is able to resolve two UCNPs with a spacing of 67 nm.

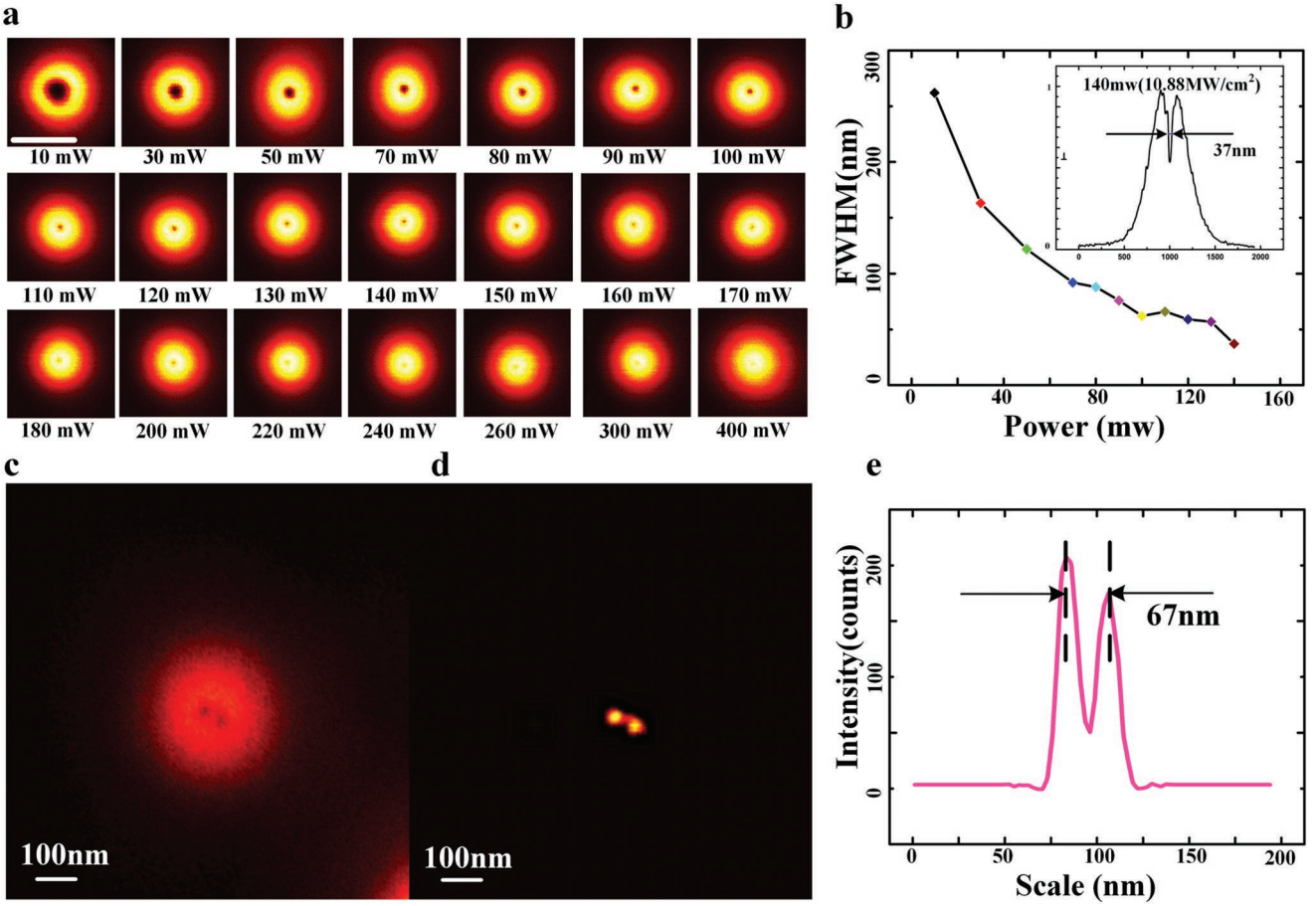

Figure 3. a) NIRB images of a single particle under different excitation power. b) The FWHM of line profiles of UCNPs from the NIRB images as a function of the excitation power. The FWHM is optimized to 37 nm with the excitation power density of 10.88 MW cm^{-2}. c) NIRB image of a pair of UCNPs. d) The positive NIRB image (NIRB+) after deconvolution and its e) cross-section profile. The spacing between the two particles is resolved as 67 nm.

We further examine the ability of NIRB nanoscopy by imaging a spheroid sample. A typical multicellular spheroid sample formed by human breast carcinoma MCF-7 cells is used in this experiment, with a diameter of around 123 µm. The cell density of spheroid is usually several times higher than conventional biological tissue (e.g., brain slide),[26,27] which result in much stronger scattering and absorption to both excitation and emission light. Hence, the spheroid is opaque under bright field illumination as shown in **Figure 4**b and Figure S6 of the Supporting Information. After 6 h incubation of the spheroid with UCNPs, we demonstrated the UCNPs mapping in 3D spheroid. We first image UCNPs with the depth of 24, 27, and 30 µm inside spheroids by confocal microscopy, NIR emission saturation nanoscopy and this NIRB nanoscopy, respectively. As shown in Figure S8 of the Supporting Information, both confocal microscopy and NIR emission saturation nanoscopy have distorted PSFs due to the strong scattering, which leads to inferior image resolution. While NIRB maintains its PSF, benefitting from good scattering control. Figure 4a shows the UCNPs mapping in the lateral plane with different depth from 0.9 to 55.9 µm inside a spheroid. It is noted that most nanoparticles are still at the periphery of the spheroid due to the relatively large particle size and short incubation time. Nevertheless, there is a sufficient amount of particles that have penetrated into the central area of the spheroid through the transcellular penetration via endocytosis and exocytosis cycles of the cells,[28–30] which indicates that 80 nm nanoparticles can be delivered to the center of a spheroid even without antibody coating. Figure 4c is the 3D reconstruction image of UCNPs in one-eighth of a spheroid by NIRB microscopy. A large amount of UCNPs is shown in the volume, with depth down to 35 µm. Figure 4d shows the 3D NIRB+ image of UCNPs in a selected cuboid volume (gray cuboid in Figure 4c), indicating its ability on quantities analysis of UCNPs inside spheroid. Figure 4e shows the small area (labeled in Figure 4a) mapping of single UCNPs by NIRB at the depth of 55.9 µm. Benefiting from its Bessel excitation beam, NIR emission, and excitation, the developed NIRB nanoscopy minimized the absorption and scattering problem in the spheroid sample, showing a super-resolution image of single UCNPs with low aberration. The crossline profiles of two labeled UCNPs are shown in Figure 4h, with the FWHM of 104 and 98 nm, respectively. To the best of our knowledge, this is the highest resolution for imaging single nanoparticles inside spheroids/organoids with depth as large as 55 µm. Figure 4f,g shows the NIRB+ images of areas of interest labeled in Figure 4e. These single particles

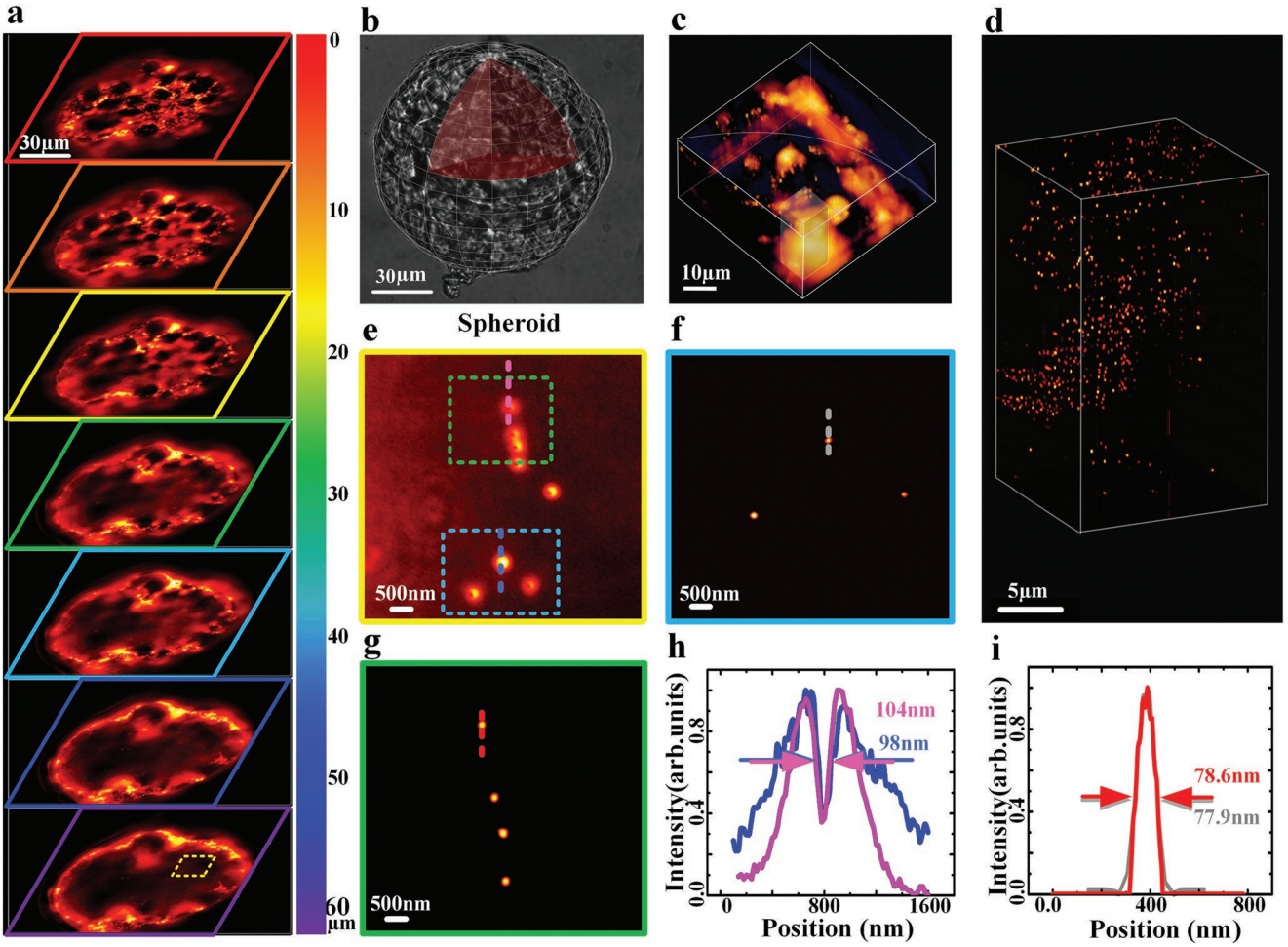

Figure 4. a) The construct *z* stack and pseudoscalar of super-resolution images of spheroid #1. b) The bright-field image of a typical spheroid cell (spheroid #1). c) The 3D NIRB image of UCNPs in one-eighth of spheroid #2. The scanning volume is 50 μm × 50 μm × 35 μm. d) The NIRB+ image of UCNPs in the selected area in (c). The scanning volume is 10 μm × 10 μm × 20 μm. e) The zoomed-in super-resolution image of UCNPs at 55.9 μm depth inside the spheroid in an outlined by the yellow rectangle. f,g) The zoomed-in view NIRB+ images of the region outlined by the green and cyan rectangle in (c). h) Cross-section profiles of UCNPs in (e) (labeled by magenta and blue line). i) Cross-section line profiles of UCNP in (g) (labeled by red) and (h) (labeled by gray). The excitation power is 8.9 MW cm^{-2}. The UCNP is doped with 40% Yb^{3+} and 4% Tm^{3+}. The pixel dwell time for confocal and NIRB is 3 ms.

images show good contrast as shown in their crossline profiles in Figure 4i.

In conclusion, we designed an NIRB nanoscopy and demonstrated that it can be used to super-resolution mapping of single nanoparticles in 3D multicellular spheroid. Under relatively low excitation power (8.9 MW cm^{-2}) of NIR excitation, the NIRB can be used to map single UCNPs with 98 nm resolution at a depth of 55.9 μm inside a spheroid. This method also enables super-resolved single nanoparticle mapping in multicellular spheroids with fast speed, such as 1 by 1 μm within 1 s. The NIRB will take 13 min to complete an image with 512 by 512 pixels, which is comparable with the imaging speed by stochastic optical reconstruction microscopy (15 min for 512 by 512 pixels).[31] Hence this method holds great potential to the monitoring of the cell uptake and transportation of nanoscale cargo in the spheroid to study the physiological responses and drug delivery process.[28] For instance, this method enables the study of penetration pathways and depth of nanoparticles with different surface polymer modification into tumor-mimicking spheroids. The finding will benefit the design of nanoparticles for improved drug delivery efficiency and enhanced therapeutic effects. Also, our imaging technology could be used for the organoid, which has similar imaging request with the spheroids. It will provide new insight into nanomedicine product design and improve the efficacy of nanodevices.

Supporting Information

Supporting Information is available from the Wiley Online Library or from the author.

Acknowledgements

The authors thank Dr. Kebin Shi for the discussion of optical simulation. The authors acknowledge financial support from the Chancellor's

Postdoctoral Research Fellowships (PRO18-6128), the University of Technology Sydney (UTS); UTS Early Career Researcher Grant (PRO17-4393), UTS; Major International (Regional) Joint Research Project of NSFC (51720105015), Shenzhen Peacock team project (KQTD20170810110913065), and Australia China Science and Research Fund Joint Research Centre for Poct (ACSRF65827), and China Scholarship Council CSC scholarships (Y.L.: No. 201607950010; C.C.: No. 201607950009; X.S.: No. 201708200004; G.F.: No. 201708140082).

Conflict of Interest

The authors declare no conflict of interest.

Keywords

deep tissue, super-resolution, tumor spheroids, upconversion nanoparticles (UCNPs)

Received: September 27, 2019
Revised: December 2, 2019
Published online:

[1] C. Willyard, *Nature* **2015**, *523*, 520.
[2] J. R. Spence, C. N. Mayhew, S. A. Rankin, M. Kuhar, E. Vallance, K. Tolle, E. E. Hoskins, V. V Kalinichenko, I. Wells, A. M. Zorn, N. F. Shroyer, J. M. Wells, *Nature* **2011**, *470*, 105.
[3] A. Fatehullah, S. H. Tan, N. Barker, *Nat. Cell Biol.* **2016**, *18*, 246.
[4] A. G. Godin, B. Lounis, L. Cognet, *Biophys. J.* **2014**, *107*, 1777.
[5] Y. Liu, Y. Lu, X. Yang, X. Zheng, S. Wen, F. Wang, X. Vidal, J. Zhao, D. Liu, Z. Zhou, C. Ma, J. Zhou, J. A. Piper, P. Xi, D. Jin, *Nature* **2017**, *543*, 229.
[6] N. De Jonge, D. B. Peckys, *ACS Nano* **2016**, *10*, 9061.
[7] F. Helmchen, W. Denk, *Nat. Methods* **2005**, *2*, 932.
[8] P. Theer, M. T. Hasan, W. Denk, *Opt. Lett.* **2003**, *28*, 1022.
[9] J. T. D. Bonis-O'Donnell, R. H. Page, A. G. Beyene, E. G. Tindall, I. R. McFarlane, M. P. Landry, *Adv. Funct. Mater.* **2017**, *27*, 1702112.
[10] S. Kukreti, A. Cerussi, B. Tromberg, E. Gratton, *Dis. Markers* **2008**, *25*, 281.
[11] M. L. Korb, J. M. Warram, J. Grudzinski, J. Weichert, J. Jeffery, E. L. Rosenthal, *Mol. Imaging* **2014**, *13*, 1.
[12] S. Karel, *Annu. Rev. Biophys. Biomol. Struct.* **1994**, *23*, 247.
[13] D. Jin, P. Xi, B. Wang, L. Zhang, J. Enderlein, A. M. van Oijen, *Nat. Methods* **2018**, *15*, 415.
[14] Q. Zhan, H. Liu, B. Wang, Q. Wu, R. Pu, C. Zhou, B. Huang, X. Peng, H. Ågren, S. He, *Nat. Commun.* **2017**, *8*, 1058.
[15] F. Wang, S. Wen, H. He, B. Wang, Z. Zhou, O. Shimoni, D. Jin, *Light: Sci. Appl.* **2018**, *7*, 18006.
[16] C. Chen, F. Wang, S. Wen, Q. P. Su, M. C. L. Wu, Y. Liu, B. Wang, D. Li, X. Shan, M. Kianinia, I. Aharonovich, M. Toth, S. P. Jackson, P. Xi, D. Jin, *Nat. Commun.* **2018**, *9*, 4.
[17] P. Bethge, R. Chéreau, E. Avignone, G. Marsicano, U. V. Nägerl, *Biophys. J.* **2013**, *104*, 778.
[18] F. O. Fahrbach, P. Simon, A. Rohrbach, *Nat. Photonics* **2010**, *4*, 780.
[19] W. Yu, Z. Ji, D. Dong, X. Yang, Y. Xiao, Q. Gong, P. Xi, K. Shi, *Laser Photonics Rev.* **2016**, *10*, 147.
[20] F. Wang, R. Deng, J. Wang, Q. Wang, Y. Han, H. Zhu, X. Chen, X. Liu, *Nat. Mater.* **2011**, *10*, 968.
[21] C. Clarke, D. Liu, F. Wang, Y. Liu, C. Chen, C. Ton-That, X. Xu, D. Jin, *Nanoscale* **2018**, *10*, 6270.
[22] C. Ma, X. Xu, F. Wang, Z. Zhou, D. Liu, J. Zhao, M. Guan, C. I. Lang, D. Jin, *Nano Lett.* **2017**, *17*, 2858.
[23] X. Xu, Z. Zhou, Y. Liu, S. Wen, Z. Guo, L. Gao, F. Wang, *APL Photonics* **2019**, *4*, 026104.
[24] E. Rittweger, D. Wildanger, S. W. Hell, *EPL (Europhys. Lett.)* **2009**, *86*, 14001.
[25] C. Kuang, S. Li, W. Liu, X. Hao, Z. Gu, Y. Wang, J. Ge, H. Li, X. Liu, *Sci. Rep.* **2013**, *3*, 1441.
[26] R. M. Sutherland, *Science* **1988**, *240*, 177.
[27] *Cancer* **1991**, *67*, 2833.
[28] H. Lu, M. H. Stenzel, *Small* **2018**, *14*, 1702858.
[29] J. Bugno, H. J. Hsu, R. M. Pearson, H. Noh, S. Hong, *Mol. Pharmaceutics* **2016**, *13*, 2155.
[30] H. Lu, R. H. Utama, U. Kitiyotsawat, K. Babiuch, Y. Jiang, M. H. Stenzel, *Biomater. Sci.* **2014**, *3*, 1085.
[31] P. Bon, J. Linarès-Loyez, M. Feyeux, K. Alessandri, B. Lounis, P. Nassoy, L. Cognet, *Nat. Methods* **2018**, *15*, 449.

